J Mater Sci: Mater Med (2010) 21:3095–3101
DOI 10.1007/s10856-010-4157-7

Spherical *N*-carboxyethylchitosan/hydroxyapatite nanoparticles prepared by ionic diffusion process in a controlled manner

Aiping Zhu · Yan Lu · Yao Zhou · Sheng Dai

Received: 9 June 2009 / Accepted: 13 September 2010 / Published online: 2 October 2010

Abstract The nanocomposites containing hydroxyapatite (HA) and biomacromolecules have attracted considerable research interest in implants, tissue scaffolds and drug controlled delivery. In this study, the *N*-carboxyethylchitosan/hydroxyapatite (NCECS/HA) nanoparticles were prepared by the ionic diffusion process in a controlled manner. The crystallization, particle size, size distribution and aggregation morphology of the NCECS/HA nanocomposites were dependent on the mole ratio of the glucosamine unit in NCECS to the Ca^{2+}. Fourier transform-infrared spectroscopic (FTIR) result indicated that there are chemical bonds formed between NCECS and HA. X-ray diffraction (XRD) analysis showed that the crystallization of HA in NCECS matrix was significantly retarded. Transmission electron microscopy (TEM) results revealed that NCECS/HA nanocomposites have the spherical morphology with the diameter ranging from 10 to 40 nm. The NCECS mineralization is driven by the self-assembly of NCECS and HA. These NCECS/HA nanocomposites have potential applications as the carrier for the controlled delivery of growth factors and drugs.

A. Zhu (✉) · Y. Lu · Y. Zhou
College of Chemistry and Chemical Engineering, Yangzhou University, Yangzhou 225002, People's Republic of China
e-mail: apzhu@yzu.edu.cn

S. Dai
School of Chemical Engineering, The University of Adelaide, Adelaide, SA 5005, Australia

1 Introduction

Hydroxyapatite (HA), $Ca_{10}(PO_4)_6(OH)_2$, is chemically similar to the mineral components of bones and hard tissues [1, 2]. HA has been reported to be osteoinductive because it can induce bone formation when being implanted in dogs [3]. The HA prepared at the nano-scale plays a crucial role in various biomedical applications due to its high surface area to volume ratio and its ultra fine structure similar to biological apatite [4, 5]. However, when particulate HA nanoparticles are mixed with saline or patient's blood, they might diffuse from the implanted site to surrounding tissues and result in the damage of healthy tissues [6]. Therefore, many polymer-based nanocomposites have been developed and used as intelligent biomaterials for tissue-engineering applications.

Natural polymers [7–9] and their derivatives [10] are widely used in biomedical technology because of their biodegradability and biocompatible characters. Chitosan (CS) is one of the important natural polymers [7] and has been used in orthopedic applications to provide temporary mechanical support to bone cells [11, 12]. Up to date, the common methods to prepare CS/hydroxyapatite (HA) composites are physical mixing and co-precipitation. For example, Yamaguchi et al. [13, 14] applied the co-precipitation method to prepare the CS/HA composites. Hu and coworkers [15, 16] reported the mineralization of CS hydrogels using an in situ hybridization approach through the ionic diffusion process in a controlled manner. Ng and coworkers developed a stepwise co-precipitation method in which the pH of the CS solution gradually increased [17] and the resulting CS/HA composite achieved the higher degree of structural organization comparing with the composites prepared by the other methods. A theoretical model, a self-assembly mechanism between CS and HA

induced by the templating effect of CS supramolecule structure, has been given to elucidate the CS mineralization process [17].

CS/HA composites are able of enhancing tissue regenerative efficacy and osteoconductivity [18, 19]. After incorporating CS, the bioactivity and the bone-bonding capability of HA could be improved significantly [20]. These CS/HA composites have been used as porous CS/HA scaffolds for tissue engineering [21] or carriers for drug controlled release [22]. They combine the tailored degradability of polymers and the osteoconductivity of ceramics. Additionally, the mechanical and physical properties of HAs such as brittleness and stiffness have been improved [23]. CS acts as the binder to avoid the migration problem after HA powder implantation. However, chitosan cannot dissolve in water at moderate pH due to the strong intermolecular hydrogen bonds, which limits its wide biomedical applications.

N-Carboxyethylchitosan (NCECS) is an amphiphilic chitosan derivative [24]. In this study, we applied a co-precipitation approach to produce NCECS/HA nanocomposite. The effects of the feed ratio of NCECS to HA on the size and morphology of NCECS/HA composites were investigated and the mechanism associated with NCECS/HA nanocomposite preparation was elucidated.

2 Experiments

2.1 Chemicals and materials

Chitosan powder was purchased from Lianyungang Biological Inc., China, which has a deacetylation degree of 90% and a viscosity average molecular weight of $\sim 2.0 \times 10^5$ g/mol. Reagent grade acrylic acid (AA) and acetone were purchased from Shanghai Chemical Plant and Nanjing Chemical Industry Co. Phosphate buffered saline (PBS) was prepared using Na_2HPO_4/NaH_2PO_4. All other chemicals were of analytical grades and used directly.

2.2 Preparation of NCECS

2.5 g chitosan powder was dissolved in the mixed solution of 125 ml distilled water and 8 ml AA monomer. It was transferred to a 250 ml three-necked flask equipped with a mechanical stirrer, a condenser and a thermometer. The reaction mixture was heated to 50°C and allowed to stir for 8 h at that temperature. After that, the mixture was cooled to room temperature and precipitated in excess amount of acetone, followed by filtration. The filtrate was washed three times using 70% acetone aqueous solution, 80% acetone aqueous solution and anhydrous acetone. The purified product was dried at 40°C under vacuum for 24 h.

2.3 Preparation of NCECS/HA nanocomposite by the ionic diffusion process in a controlled manner

The recipes to prepare NCECS/HA nanocomposites were given in Table 1. In the nanocomposite nomenclature of NCECS/HA-X, the value X of 20, 40, 60 and 80 represents the HA feed percentage during the course of nanocomposite preparation. In a typical experiment, NCECS powders were dissolved in 40 ml distilled water, and the solution was charged to a 100 ml glass reactor. 20 ml $(Ca(NO_3)_2)\cdot 4H_2O$ aqueous solution was added under vigorous agitation to obtain a homogeneous mixed solution. The temperature was risen to 35°C, and 10 ml of KH_2PO_4 aqueous solution was added drop-by-drop. After that, the reaction mixture was maintained at 35°C for 6 h. The obtained transparent solution was transferred to a dialysis bag (molecular weight cut-off 12000–14000 Da), and the sealed dialysis bag was soaked into 100 ml of alkaline aqueous solution (pH $\sim$ 12, adjusted by 1 M NaOH solution). The dialysis system was put in a 37°C shaking bath for about 6 h for the co-precipitation reaction. The obtained suspension was centrifuged at 20,000 rpm for 10 min. The NCECS/HA nanocomposites were obtained by freeze-drying.

2.4 Characterization of NCECS/HA composites

FTIR spectra were recorded using a Biorad FTS 6000 spectrophotometer using KBr pellets. The phases of nanocomposite powders were analyzed by an X-ray diffractometer (D/MAX-2500) with Cu Kα radiation at 40 kV and 100 mA. Specimens were scanned in the range of $10° < 2\theta < 60°$, and each experiments were repeated for at least three times. The thermal degradation behavior was studied using a thermal gravimetric analyzer (TGA) (STA 409PC, Germany NETZSCH company). Small amount of powder samples (5–8 mg) were loaded to an alumina pan and heated to 100°C, held for 5 min to remove residual moisture, and then heated from 100 to 1000°C at a constant rate of 10°C/min under atmosphere. The sizes and size distributions of nanocomposites were determined using dynamic light scattering (DLS) (ALV/SP-125, Germany), equipped with a 400 mW 532 nm solid-state laser (Coherent

Table 1 Receipt for the preparation of different compositions

Samples	$Ca(NO_3)_2\cdot 4H_2O$ (g)	$(NH_4)_2HPO_4$ (g)	NCECS (g)
NCECS/HA-20	1.2068	0.2160	1.1294
NCECS/HA-40	0.5600	0.1015	0.1905
NCECS/HA-60	0.6705	0.1206	0.1008
NCECS/HA-80	1.2068	0.2160	0.0685

DPSS) and an ALV-5000 multi-τ digital time correlator. For DLS experiments, each measurement was repeated for at least three times. Morphological studies on the nanocomposites were conducted using a TE CHAI-12 (Philips) transmission electron microscopy (TEM). The zeta potentials of the nanocomposites were examined using a zeta-potential analyzer (Zetaplus, Brookhaven Instruments).

3 Results and discussion

3.1 FTIR

The synthesis of NCECS is described in Scheme 1. From our previous work [24], the degree of carboxyethyl group substitution in the NCECS was ~41.7% based on ^{1}H NMR measurement. Figure 1 compares the FTIR spectra of (a) NCECS and (b) NCECS/HA-60 nanocomposite. In the spectrum of NCECS, distinctive absorption bands appear at: 3446 cm^{-1} (N–H stretch); 1652 cm^{-1}, which denotes the acetylated amino group (amide I) of chitin and thus indicates the chitosan used is partially deacetylated; 1569 cm^{-1} (amide II and COOH); 1404 cm^{-1} (CH_2 (in $-CH_2CH_2COOH$) stretch), and 1075 cm^{-1} (skeletal vibration involving the C–O stretch). The above result proves the successful carboxyethyl substitution on the amino groups of chitosan. The FTIR spectrum of NCECS/HA-60 composite is depicted in Fig. 1b, where the broad OH stretching band in 3550–3350 cm^{-1} and the aliphatic CH stretching band in 2996–2882 cm^{-1} are evident. The phosphate groups of HA appears at the wavenumbers of 1033, 603 and 571 cm^{-1}. In addition, comparing with NCECS, the peak at 1569 cm^{-1} (amino and carboxyl group characteristic peak) shifts to 1576 cm^{-1}, while the intensity decreases significantly. Such result suggests the formation of chemical bonds between NCECS and HA.

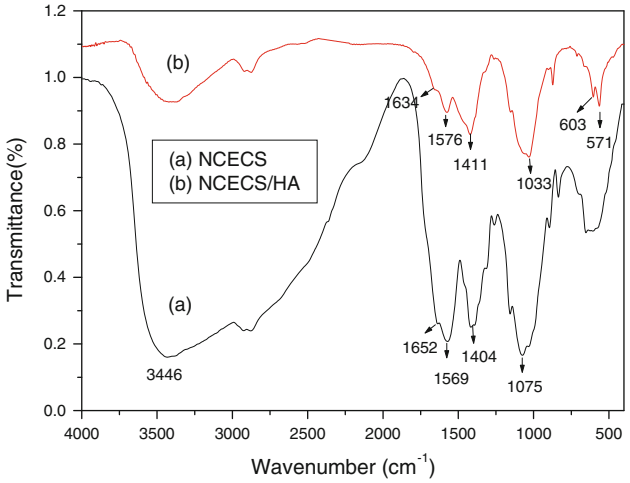

Fig. 1 FTIR spectra of (*a*) NCECS and (*b*) NCECS/HA-60 nanocomposites

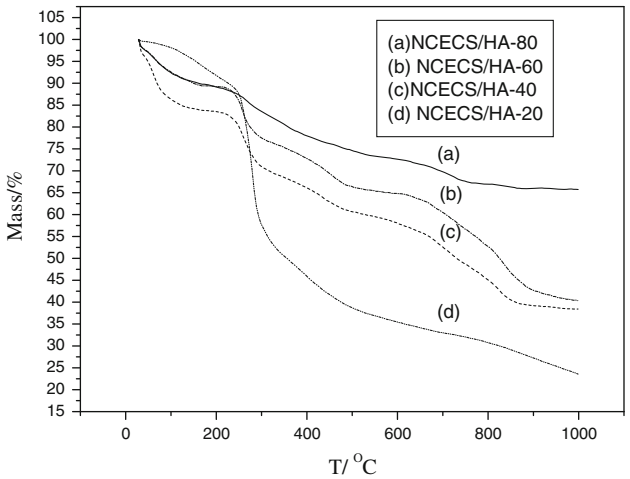

Fig. 2 The TGA thermograms of various NCECS/HA nanocomposites

3.2 Thermogravimetric analysis (TGA)

The TGA thermograms of various NCECS/HA composites are shown in Fig. 2, and there are two continuous weight losses in the temperature ranges of 70–150 and 210–600°C. The former is associated with the loss of moisture and the latter is attributed to thermal decomposition of NCECS. Although there is no significant difference in the shapes of decomposition thermograms for various NCECS/HA nanocomposites, the percentage of weight loss increases with increasing the mole ratio of glucosamine in NCECS to Ca^{2+}. In detail, the total weight losses are found to be 34.0, 59.0, 61.6 and 77.2 wt% for NCECS/HA-80, NCECS/

Scheme 1 Synthesis schemes of NCECS and HA

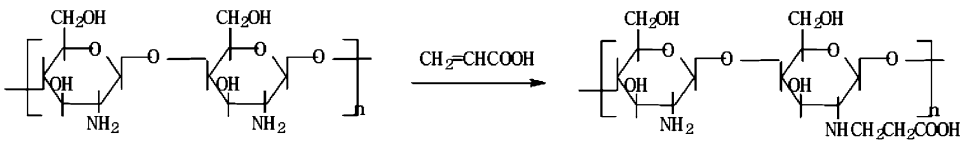

$$10\,Ca^{2+} + 6\,H_2PO_4^- + 14\,OH^- \longrightarrow Ca_{10}(PO_4)_6(OH)_2 + 12H_2O \quad (pH > 10)$$

Table 2 Comparison on the feed and the measured HA percentage (based on TGA) for various NCECS/HA nanocomposites

Sample name	Measured	Feed
NCECS/HA-20	22.8	20
NCECS/HA-40	38.4	40
NCECS/HA-60	41.0	60
NCECS/HA-80	66.0	80

HA-60, NCECS/HA-40 and NCECS/HA-20. Additionally, there is almost no weight loss after 800°C for all nanocomposites, which indicates that all organic moieties have been decomposed below 800°C. The HA content and the HA conversion determined from TGA experiments are listed in Table 2. We can find that the HA conversion decreases with decreasing the mole ratio of glucosamine in NCECS to Ca^{2+}. Obviously, above TGA results confirm the successful preparation of polymer/ceramic composite materials.

3.3 Morphology of NCECS/HA nanocomposites

TEM micrographs of NCECS/HA nanocomposites are shown in Fig. 3. Figure 3a is the TEM image of NCECS/HA-80 which has the lowest mole ratio of glucosamine in NCECS to Ca^{2+}. Regular spherical morphology with an average diameter of 20–30 nm is observed. These particles tend to self-assemble to secondary clusters with grape-like morphology. For NCECS/HA-60 (Fig. 3b), the nanocomposite shows well-dispersed spherical morphology with a uniform diameter of 20 nm. However, the morphology of NCECS/HA-40 nanocomposite is totally different from that of NCECS/HA-60 or NCECS/HA-80. Small particles, with an average diameter of 15–20 nm, assemble to spheres with a diameter ranging from 80 to 150 nm (Fig. 3c). The presence of large compound aggregation for NCECS/HA-40 nanocomposites agrees with previous studies by Ng and coworkers [17], where stepwise co-precipitation approach was used to prepare CS/HA nanocomposites. They found the bimodal distribution of

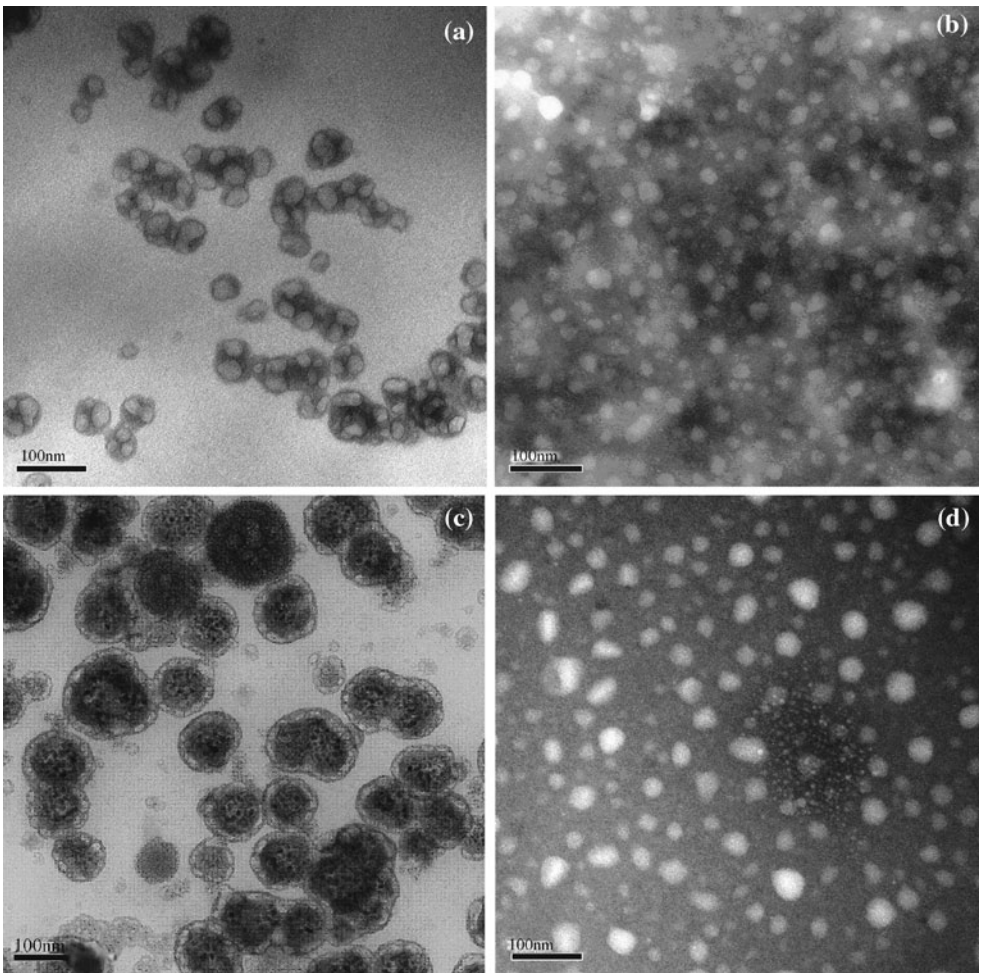

Fig. 3 TEM images of NCECS/HA nanocomposites: **a** NCECS/HA-80; **b** NCECS/HA-60; **c** NCECS/HA-40; **d** NCECS/HA-20

nano-scaled hydroxyapatite in chitosan matrix, where the cluster-like aggregates (between 200 and 400 nm) were the habitat of "small" (between 7 and 18 nm) hydroxyapatite nanocrystallites and the scattered-like aggregates were the habitat of "large" (between 25 and 45 nm) hydroxyapatite nanocrystallites. The NCECS/HA-20 demonstrates a well-dispersed spherical morphology with a diameter of 20–40 nm (Fig. 3d). The morphological study clearly demonstrates that the particle sizes, size distributions and aggregation morphologies of NCECS/HA nanocomposites are dependent on the feed mole ratio of glucosamine in NCECS to Ca^{2+}. Additionally, all these synthesized HA nanocomposites are within the range of biological HA size.

3.4 Crystalline phase(s) of NCECS/HA nanocomposites

The typical XRD patterns of pure HA (prepared in our lab) and NCECS/HA nanocomposites are compared in Fig. 4. All diffraction peaks of HA are well defined.

The XRD pattern of NCECS/HA-80 composite consists of broad bands, indicating the solid phase appears as very small crystallites and/or as a disordered state (low crystallinity). Small HA crystals with a relatively low crystallinity are similar to natural bone [25, 26]. On the other hand, in the pattern of NCECS/HA-20 composite, not only the diffraction characteristic peaks of HA monophase crystalline but also a broad peak is observed at approximate 20°, which is attributed to NCECS. Additionally, the sharp diffraction at ~29.4° is the characteristic peak of β-calcium phosphate. The XRD results indicate that other calcium phosphate phases are formed in NCECS/HA-20 nanocomposites. In summary, the crystallinity and the inorganic phase content of NCECS/HA nanocomposites are dependent on the feed mole ratio of glucosamine in NCECS to Ca^{2+}.

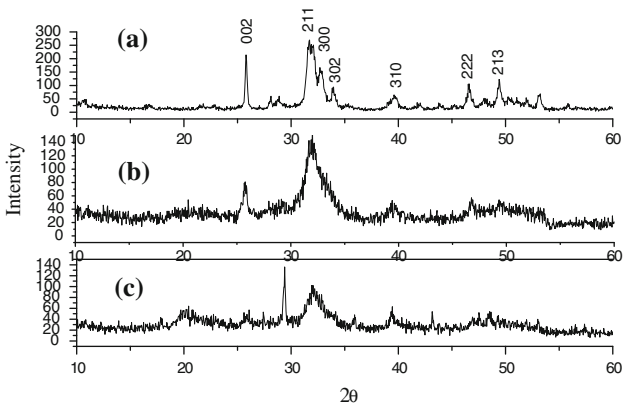

Fig. 4 XRD patterns of **a** HA, **b** NCECS/HA-80 and **c** NCECS/HA-20

3.5 Dispersibility of NCECS/HA nanocomposites in aqueous system

The aqueous suspensions of NCECS/HA nanocomposites are transparent and stable, indicating their good dispersibility in aqueous system. This is attributed to the amholytical character and the chemical structure of NCECS. The hydrodynamic radius distributions of NCECS/HA nanocomposites at a measurement angle of 90° are shown in Fig. 5. The mean hydrodynamic radius and the polydispersity index from DLS measurements are summarized in Table 3. The average hydrodynamic radius of NCECS/HA nanocomposites ranged from 250 to 330 nm, which is much larger than those from TEM, which is attributed to the solvation of NCECS/HA nanocomposites in aqueous media.

The electrophoresis of NCECS/HA nanocomposite suspensions show relatively low zeta potential values (<5 mV) (Fig. 6). Based on DLVO theory, such low zeta-potential values are not enough to stabilize these synthesized NCECS/HA nanocomposites. Therefore, it could be concluded that the sterically hindrance from solvated hydrophilic moieties such as amino, hydroxyl, carboxyl

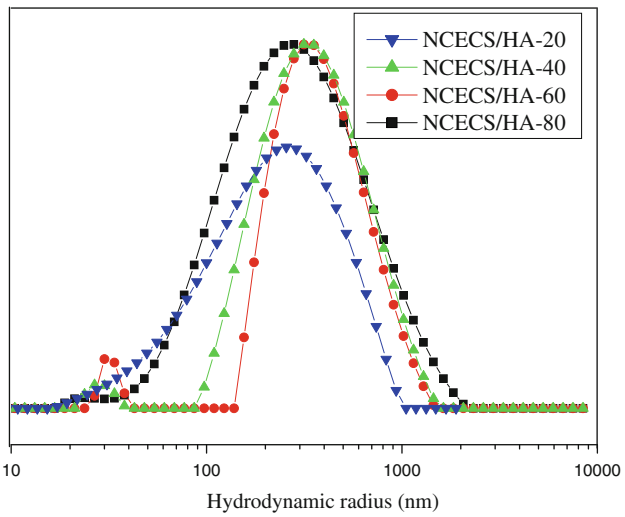

Fig. 5 The hydrodynamic radius distributions of NCECS/HA nanocomposites (dispersed in distilled water) at a scattering angle of 90°

Table 3 The hydrodynamic radius and polydispersity index of various NCECS/HA nanocomposites measured by DLS

Sample name	NCECS/HA-20	NCECS/HA-40	NCECS/HA-60	NCECS/HA-80
Hydrodynamic radius (nm)	260 ± 23	330 ± 31	325 ± 19	252 ± 17
Polydispersity index	0.28 ± 0.02	0.15 ± 0.01	0.17 ± 0.01	0.23 ± 0.02

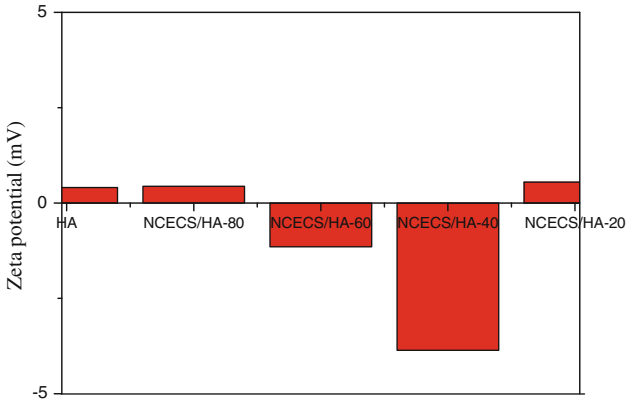

Fig. 6 The zeta potential of NCECS/HA nanocomposites (dispersed in distilled water)

groups in NCECS is the decisive factor to stabilize NCECS/HA nanocomposite in aqueous media. The good suspension/colloid stability is the basic requirement for developing NCECS/HA nanocomposite applications in drug controlled release and gene delivery.

3.6 The mechanism for NCECS/HA nanocomposite preparation

NCECS is water-soluble in a broad pH range. In acidic solution, NCECS is soluble due to the protonation of the amino groups of NCECS (NCECS–NH_3^+); in neutral pHs, NCECS is soluble due to the presence of *N*-carboxyethyl substitution and the OH groups of glucosamines; in alkaline solutions, NCECS is able to dissolve in water because of the neutralization of the carboxyl groups of NCECS (NCECS–COO^-). For biological application purpose, we focus on investigating NCECS/HA nanocomposites in neutral aqueous media.

During the course of NCECS/HA nanocomposite preparation, a cylindrical dialysis bag was used to obstruct NCECS and achieve the ionic diffusion process in a controlled manner (Scheme 2). Small ions, such as OH^-, Ca^{2+}, $H_2PO_4^-$, are able to pass through the dialysis membrane induced by their concentration gradients until their concentrations become uniform. Inside the dialysis bag, Ca^{2+} and $H_2PO_4^-$ ions incorporate with NCECS due to their interaction between the carboxyl and amino groups of NCECS. When OH^- (A) ions encounter NCECS together with Ca^{2+} and $H_2PO_4^-$ in the dialysis bag, NCECS/HA nanocomposites are formed (Scheme 2). The carboxyl groups in NCECS are the active sites for coordinating Ca^{2+} to form the nano-complexes, which act as the active sites for nucleation. As a result, chemical bonds are formed between inorganic (HA) and organic (NCECS) phases, which is confirmed by FTIR spectrum.

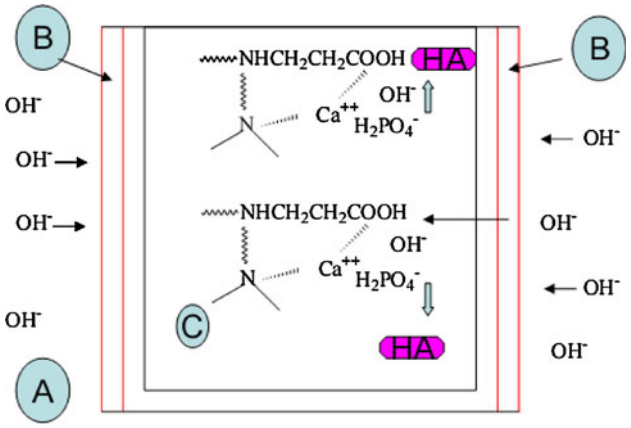

Scheme 2 The schematic representation for the mechanism of synthesizing NCECS/HA nanocomposites through in situ precipitation method. (*A*) 0.01 M sodium hydroxyl aqueous solution; (*B*) dialysis bag; (*C*) NCECS solution containing Ca^{2+} and $H_2PO_4^-$

For the reaction with a low mole ratio of glucosamine in NCECS to Ca^{2+}, NCECS is not able to integrate all Ca^{2+} and $H_2PO_4^-$. Therefore, some Ca^{2+} and $H_2PO_4^-$ ions emigrate to the aqueous solution (A) outside the dialysis bag and form HA. This is the reason that the HA conversion depends on the feed mole ratio of glucosamine in NCECS to Ca^{2+} (Table 2). In summary, the self-assembly between NCECS and HA induced by the templating effect of amphiphilic NCECS supramolecular structures [24] drives the NCECS mineralization process. The self-assembly behavior tailored by the molar ratio of glucosamine in NCECS to Ca^{2+} controls the architecture (sizes, size distributions and aggregation morphologies) of the resulting NCECS/HA nanocomposites (Fig. 3). In addition, the synthesized NCECS/HA nanocomposites, containing many active amino and carboxyl groups, provide great potential to immobilize bioactive molecules used for drug/gene delivery system.

4 Conclusions

In this study, various spherical NCECS/HA nanocomposites, with their diameters ranging from 10 to 40 nm, were prepared by ionic diffusion processes in a controlled manner. The nanocomposite suspensions show good stability in neutral aqueous solution, and the stabilization mechanism is attributed to the sterically hindrance produced by the hydrophilic moieties such as amino, hydroxyl, and carboxyl groups in NCECS. The sizes, size distributions and aggregation morphologies of nanocomposites could be tailored by changing the feed mole ratio of glucosamine in NCECS to Ca^{2+}. The self-assembly between NCECS and HA induced by the templating effect of the amphiphilic NCECS supramolecular structures drives

the NCECS mineralization process. Such NCECS/HA nanocomposites have potential applications in biomedical fields such as drug controlled release and gene delivery.

Acknowledgments This research was supported by a National Natural Science Foundation of China (No. 51073133), a Natural & Scientific Grant of Jiangsu Province, Project No. BK2006072 (China), and a Project No. 08KJA430003 (China).

References

1. Tao JH, Pan YW, Xu XR, Tang RK. Roles of amorphous calcium phosphate and biological additives in the assembly of hydroxyapatite nanoparticles. J Phys Chem B. 2007;111:13410–8.
2. Sabokbar A, Pandey R, Diaz J, Quinn JMW, Murray DW. Hydroxyapatite particles are capable of inducing osteoblast formation. J Mater Sci: Mater Med. 2001;12:659–64.
3. Yuan H, Yang Z, Zhang X, De Bruijin JD, de Groot K. Osteoinduction by calcium phosphate biomaterials. J Mater Sci: Mater Med. 1998;9:723–6.
4. Webster TJ, Siegel RW, Bizios R. Enhanced functions of osteoblasts on nanophase ceramics. Biomaterials. 2000;21:1803–10.
5. Elliot JC. Structure, chemistry of the apatites and other calcium orthophosphates, vol. 111. Amsterdam: Elsevier; 1994.
6. Miyamato Y, Shikawa KI. Basic properties of calcium phosphate cement containing atelocollagen in its liquid or powder phases. Biomaterials. 1998;19:707–15.
7. Grodzinski JJ. Biomedical applications of functional polymers. React Fuct Polym. 1999;39:99–138.
8. Burg KJL, Porter S, Kellam JF. Biomaterial developments for bone tissue engineering. Biomaterials. 2000;21:2347–59.
9. Hutmacher DW. Scaffold in tissue engineering bone and artilage. Biomaterials. 2000;21:2529–43.
10. Chang MC, Tanaka J. XPS study for the microstructure development of hydroxyapatite-collagen nanocomposites cross-linked using glutaraldehyde. Biomaterials. 2002;23(18):3879–85.
11. Lee JY, Nam SH, Im SY, Park YJ, Lee YM, Seol YJ, Chung CP, Lee SJ. Enhanced bone formation by controlled growth factor delivery from chitosan-based biomaterials. J Control Release. 2002;78(1–3):187–97.
12. Eugene K, Lee YL. Inplantable application of chitin and chitosan. Biomaterials. 2003;24:2339–49.
13. Yamaguchi I, Tokuchi K, Fukuzaky H, Koyama Y, Takakuda K, Momna H, Tanaka J. Preparation and mechanical properties of chitosan/hydroxyapatite nanocomposites. Key Eng Mater. 2001; 192–195:673–6.
14. Yamaguchi I, Tokuchi K, Fukuzaky H, Koyama Y, Takakuda K, Momna H, Tanaka J. Preparation and microstructure analysis of chitosan/hydroxyapatite nanocomposites. J Biomed Mater Res. 2001;55:20–7.
15. Beppu MM, Santana CC. In vitro biomineralization of chitosan. Key Eng Mater. 2001;192–195:31–4.
16. Hu Q, Li B, Wang M, Shen J. Preparation and characterization of biodegradable chitosan/hydroxyapatite nanocomposite rods via in situ hybridization: a potential material as internal fixation of bone frature. Biomaterials. 2004;25(5):779–85.
17. Rusu VM, Ng CH, Eilke M, Tiegitte B, Fratzl P, Peter MG. Size-controlled hydroxyapatite nanoparticles as self-organized organic-inorganic composite materials. Biomaterials. 2005;26: 5414–26.
18. Ito M. In vitro properties of a chitosan-bonded hydroxyapatite bone filling past. Biomaterials. 1991;12:41–451.
19. Kawakami T, Antoh M, Hasegawa H, Yamaguchi I, Ito M, Eda S. Experimental study on osteoconductive properties of chitosan-bonded hydroxyapatite self-hardening paste. Biomaterials. 1992; 13(11):759–63.
20. Wang XH, Ma JB, Wang YN, He BL. Bone repair in radii and tabias of rabbits with phosphorylated chitosan reinforced calcium phosphate cements. Biomaterials. 2002;23:4167–76.
21. Zhang Y, Zhang MO. Synthesis and characterization of macroporous chitosan/calcium phosphate composite scaffolds for tissue engineering. J Biomed Mater Res. 2001;55(3):304–12.
22. Zhang Y, Zhang MQ. Calcium phosphate/chitosan composite scaffolds for controlled in vitro antibiotic drug release. J Biomed Mater Res. 2002;62(3):378–86.
23. Muzzarelli C, Muzzarelli RAA. Natural and artificial chitosan-inorganic composites. J Inorg Biochem. 2002;92:89–94.
24. Pan YN, Luo XD, Zhu AP, Dai S. Synthesis and physicochemical properties of biocompatible N-carboxyethylchitosan. J Biomater Sci Polym Ed. 2009;20:981–92.
25. Murugan R, Ramakrishna S. Bioresorbable composite bone paste using polysaccharide based nano hydroxyapatite. Biomaterials. 2004;25:3829–35.
26. Rhee SH, Tanaka J. Self-assembly phenomenon of hydroxyapatite nanocrystals on chondroitin sulfate. J Mater Sci: Mater Med. 2002;13:597–600.